Int J Thermophys (2016) 37:85
DOI 10.1007/s10765-016-2091-8

ICPPP 18

Long-Wave Infrared Thermophotonic Imaging of Demineralization in Dental Hard Tissue

A. Ojaghi[1] · A. Parkhimchyk[1] · N. Tabatabaei[1]

Received: 9 October 2015 / Accepted: 11 June 2016 / Published online: 6 July 2016

Abstract Dental caries remains the most prevalent chronic disease in both children and adults worldwide. To address this prevalence through disease prevention and management, dentists need tools capable of detecting caries at early stages of formation. Looking into the physics of light propagation in teeth, this study presents a clinically and commercially viable platform technology for thermophotonic detection of early dental caries using an inexpensive long-wavelength infrared (LWIR; 8 μm to 14 μm) camera. The developed system incorporates intensity-modulated light to generate a thermal-wave field inside enamel and uses the subsequent infrared emission of the thermal-wave field to detect early caries. It was found that the greater light absorption at caries sites shifts the thermal-wave field centroid, providing contrast between early caries and intact enamel. Use of LWIR detection band in dental samples is novel and beneficial over the conventional mid-wavelength infrared band (3 μm to 5 μm) as it suppresses the masking effect of the instantaneous radiative emission from subsurface features due to the minimal transmittance of enamel in the LWIR band. The efficacy of the LWIR system is verified though experiments carried out on nonbiological test samples as well as on teeth with natural and artificially induced caries. The results suggest that the developed LWIR technology is an affordable early dental caries detection system suitable for commercialization/translation to Dentistry.

Keywords Controlled demineralization · Early dental caries · Lock-in thermography · Long-wavelength infrared · Thermophotonic lock-in imaging

This article is part of the selected papers presented at the 18th International Conference on Photoacoustic and Photothermal Phenomena.

✉ N. Tabatabaei
nima.tabatabaei@lassonde.yorku.ca

[1] Department of Mechanical Engineering, York University, Toronto M3J 1P3, Canada

1 Introduction

Development of new methods for detection of dental caries, particularly in early stages of formation, has been the focus of a great number of research projects in the recent years. Dental caries is a chronic disease identified as the most prevalent dental disease among children and adult populations and is the leading cause of tooth loss. The precursor of the disease is a minute amount of mineral loss (demineralization) from the enamel surface as a result of decomposition of hydroxyapatite crystals in the acidic environment [1]. Such early caries can turn into a cavity if given enough time in the acidic environment of dental plaques. The significance of early caries detection lies in the fact that if dental caries are detected in their early stages of formation, preventive actions, such as oral hygiene counseling or fluoride therapy [2], can be used not only to prevent the caries from turning into a cavity, but also, to heal (i.e., remineralize) them. Unfortunately, the conventional clinical diagnostic modalities, such as X-ray radiography and visual/tactile inspections, lack sufficient sensitivity and specificity to detect early caries [3].

Optical methodologies have shown great potential for early detection of dental caries. The source of contrast in these methods is the intrinsic difference between optical properties (e.g., absorption or scattering) of the sound and demineralized tissues. Accordingly, a number of different optical methods such as the fiber-optic transillumination (FOTI) [4] have been developed for caries detection. FOTI uses high-intensity white light for detecting caries. However, due to the significant scattering of light in the visible spectrum, inconsistent results have been reported, suggesting poor sensitivity of this method due to the masking effect of background signal originating from the healthy tissue surrounding the malignancy. Near-infrared (NIR) transmission/reflectance methods work on the same basis as FOTI but use near-infrared light instead of visible light to gain deeper penetration in dental hard tissues as a result of reduced scattering and absorption of enamel in the NIR region. The main disadvantage of these methods is the poor detection specificity to very early demineralization as the source of diagnostic contrast in these methods is the enhanced light scattering within the carious regions which can effectively be masked by the surrounding intact tissues and the anisotropic structure on dentin. Although promising results have been reported for caries detection through NIR transmission/reflectance methods [5–7], their application in clinical diagnosis appears to be limited.

Optical coherence tomography (OCT) is another imaging modality, capable of imaging the tissue microstructure within the caries lesions. OCT works based on illumination of the tissue via a NIR light, collection of backscattered light, and analysis of the light intensity as it interfered with a reference light beam. The intensity of the interference is dependent upon the scattering caused by structural changes in the dental tissue [8]. A number of studies have demonstrated the ability of OCT in detection of demineralization in enamel *in vitro* through changes in the tissue reflectivity [9]. However, image artifacts caused by interfering effect of intact tissues surrounding the malignancies with the backscattered light from carious regions, loss of coherence for deep zone imaging due to extreme light scattering, and high equipment cost prohibit the clinical adaptation of dental OCT [10].

Another group of optical methodologies, known as energy conversion methods, works based on transformation of optical energy to other energy forms. Quantitative light-induced fluorescence (QLF) is one such method working based on light-to-fluorescence conversion and the decrease in fluorescence transmission due to increased scattering from demineralized spots. In QLF, fluorescence is caused by the excitation of fluorophores contained within the enamel–dentin junction using visible light. Although QLF is capable of detecting early carious lesions [11], the need for extensive operator training and the masking effects of surface stains hinder the applicability of this technique in real-world clinical scenarios.

Thermophotonic lock-in (TPLI) imaging is an alternative optical method used for dental caries detection. This form of detection belongs to the energy conversion methodologies and uses the thermal infrared (Planck) radiation from teeth to detect carious lesions. TPLI uses diffusive thermal waves as markers to gather information about subsurface characteristics of tooth structures. In this method, a low-power, continuous, and intensity-modulated light source (e.g., laser) is utilized to generate a thermal-wave field inside the tooth and the subsequent infrared emission of the thermal wave field is used to detect caries. That is, the local surface temperature modulation is evaluated and averaged over a number of cycles, while the heat is introduced to the sample periodically at a certain lock-in frequency. The use of lock-in principle is to evaluate the alternating (ac) part of the detected signal which carries information from subsurface inhomogeneities. Subsurface defects alter the local centroid of the thermal-wave field, causing them to appear differently from the sound regions. As such, lock-in demodulation of the thermophotonic signal leads to calculation of phase and amplitude images based on the reference signal (i.e., optical excitation modulation signal).

John and Salerno [12] and John et al. [13] were among the first who used lock-in thermography for medical diagnosis. They examined the ground section of a resin-embedded extracted human tooth using modulated optical excitation and lock-in thermography. However, the result of their study is limited only to estimation of the relative thermal thicknesses of several structures and no diagnostic study was carried out due to use of highly scattering visible light as the optical excitation source and very low modulation frequencies (0.06 Hz to 0.23 Hz). In a more recent study, Tabatabaei et al. [14] used lock-in thermography for imaging of demineralization in dental tissues using a research-grade MWIR camera. The study demonstrated the great potential of TPLI for resolving dental caries at very early stages of formation; however, the camera used in this study was an expensive ($75 k) research-grade camera with integrated cryogenic cooling system not suitable for commercialization/translation to Dentistry.

Development of commercially viable medical diagnostic devices with reasonable sensitivity has always been a challenge. Recent advances in the field of microelectronics has enabled the design and manufacture of long-wave infrared (LWIR) microbolometer detector arrays which does not require integrated cryogenic cooling systems, reducing both the size and overall cost of the IR cameras. Although these infrared cameras are currently being utilized for different industrial applications such as, nondestructive evaluation of materials [15–18], there exist a great number of potential opportunities for their use in the medical sciences (such as dental early caries detection) for development of economically viable clinical diagnostic systems.

As such, to effectively translate the TPLI technology to Dentistry, a low-cost LWIR camera can potentially be used in the system.

Use of long-wave infrared (LWIR) detection band, instead of the conventional mid-wavelength infrared (MWIR) band, is beneficial for interrogation of samples at room temperature as for these samples the peak of the black body radiation falls in the LWIR band (i.e., considerably more LWIR photon flux). A larger energy flux entails that the detector can absorb a larger quantity of photons during the camera frame integration time and, consequently, a larger output signal is produced by the IR detector. However, the sensitivity of a cryogenic MWIR detector is higher than that of an uncooled microbolometer LWIR detector; yet, for samples at or near room temperature, the higher energy flux in the LWIR band is expected to alleviate the inferior sensitivity. Aside from affordability and detection sensitivity, LWIR detection in dental samples is novel and beneficial from the thermal-wave science point of view as the direct Plank emission (radiative heat transfer) from subsurface thermal sources (e.g., early caries) is effectively suppressed in this region due to the minimal optical transmittance of enamel (enamel transmittance: MIR = 75 %, LWIR = 7 % [7]), producing only conductive thermal-wave images in the camera [19].

Despite the ubiquitous integration of LWIR detectors in industrial nondestructive evaluation of materials [15–18], there exists no active LWIR thermography study in the medical sciences. As such, the overarching goal of this research, as the first biomedical active thermography research in the LWIR band, is to incorporate the LWIR technology along with lock-in signal processing technique to translate the previously developed dental MWIR technology [14] into Dentistry as a clinically and commercially viable device. In what follows, the viability of the LWIR TPLI system is demonstrated though experimental investigations performed on biological and nonbiological samples.

2 Experimental Apparatus and Procedures

2.1 Experimental Setup

The experimental setup used in this study (Fig. 1) consists of a continuous wave 808 nm near-infrared laser (Jenoptik, Jena, Germany) to which a multimode optical fiber with core diameter of 200 μm is coupled. A laser controller unit (Ostech, Berlin, Germany) is used to thermally stabilize the laser and modulate its intensity. The modulated laser

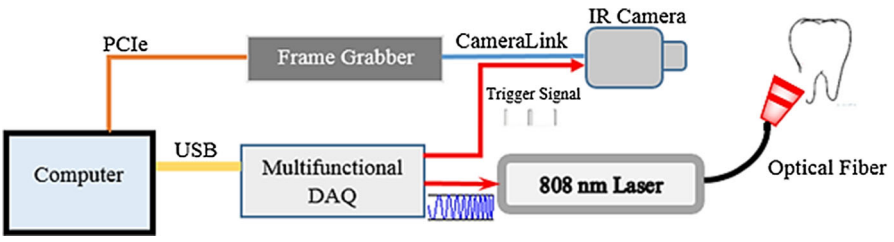

Fig. 1 Schematic of the experimental setup consisting of a NIR 808 nm laser, a LWIR camera, a frame grabber, and a multifunctional DAQ device for signal modulation and system synchronization

beam illuminates the sample through the optical fiber. In order to have a beam with uniform optical intensity over the interrogated area, a collimator (Thorlabs, Newton, NJ, USA, F220SMA-780) is used to obtain a constant beam size in conjunction with an optical diffuser (Thorlabs, Newton, NJ, USA, ED1-C20-MD).

A low-cost LWIR camera ($\sim$ \$6 K) (Xenics, Leuven, Belgium) with Cameralink type connection, spectral range of 8 μm to 14 μm, and maximum frame rate of 50 fps is focused on the surface of a LEGO-mounted sample. The sample is placed on a rotation stage mounted on a three-axis XYZ translation stage (precision 10 μm). A custom-made extension tube along with an 18 mm focal-length objective lens (Xenics OPT-000179) is used to obtain a magnification of unity (1) from the interrogated surface of the sample. A frame grabber (Euresys, Angleur, Belgium, Grablink Full) sends the captured images from the camera to the computer. The multifunctional data acquisition board (National Instruments, Austin, TX, NI USB-6363 BNC) synchronously generates three analog outputs: trigger pulse train, in-phase, and quadrature reference signals. The laser controller modulates the intensity of the laser beam based on the in-phase reference signal.

A computer program, designed in LabView environment, captures the images at a specified rate and at the same time records the corresponding values of in-phase and quadrature signals. The program weights and averages the images using the instantaneous readings of the two reference signals. Then the weighted frames are summed to obtain the low-pass filtered in-phase (S^0) and quadrature (S^{90}) images. The amplitude and phase images are then calculated by applying (Eq. 1) to each pixel:

$$A = \sqrt{(S^0)^2 + (S^{90})^2} \quad \text{and} \quad \varphi = \arctan\left(\frac{S^{90}}{S^0}\right). \tag{1}$$

2.2 Synchronous Undersampling

One of the main limitations of inexpensive infrared cameras is the low frame rate (e.g., maximum of 50 Hz for the LWIR camera used in this study), limiting its use to monitor high-frequency phenomena. Typically, for reliable retrieval of amplitude and phase information of signals, a minimum of $n = 4$ samples per modulation cycle is required [20]. To overcome this limitation in our LWIR TPLI system, for modulation frequencies above 5 Hz, the LabView data acquisition program is designed based on the synchronous undersampling method in which the required "n" samples are captured from "n" consecutive cycles instead of one [20]. Using this method, the developed system can reliably interrogate dental samples at optical modulation frequencies of up to 1 kHz.

2.3 Samples

To evaluate the capabilities of the imaging system, a number of biological and nonbiological samples are used in this study. An aluminum block with three 5 mm diameter blind holes, located at various depths from the surface, was prepared to simulate an opaque sample with defects at several depths. The holes were drilled to give wall thick-

nesses of 200 μm, 500 μm, and 1500 μm. The interrogated side of the sample is painted with a matt black color to enhance the optical absorption on the surface. In addition, a number of dental samples (extracted teeth) were obtained and the healthy-looking ones, with no visible stain or white spot lesion, were selected to study the controlled progression of demineralization with time. Samples suspected to have caries, were used in their natural state to evaluate the performance of our imaging system in diagnostic scenarios encountered in clinical practice. After preliminary visual inspection, the samples are cleaned and mounted on LEGO blocks using an epoxy adhesive. This allows the samples to be remounted in the same position in the experimental setup during repeated measurements.

2.4 Controlled Demineralization Protocol

Controlled demineralization is applied on dental samples using a lactic acid-based solution. The solution is an acidified gel, consisting of 0.1 M lactic acid and 0.1 M NaOH, gelled with addition of 6 % w/v hydroxyethylcellulose. The aim of controlled demineralization in the current study is to see the contrast between demineralized and healthy areas during different stages of caries formation. To this end, a treatment protocol is followed in a time-dependent experiment in which the tooth surface is covered with transparent nail polish except for a 2.5 mm (W) × 5 mm (H) rectangular window (i.e., treatment window). The demineralization on the window is carried out by submerging the sample upside down in a test tube containing 20 ml of demineralizing gel. After application of treatment for two days, the sample is removed from the gel, cleaned by rinsing under running water, and dried in air. Then, the transparent nail polish is removed from the interrogated surface with acetone and the sample is again rinsed and air dried before TPLI. After the imaging, the sample is again covered with the transparent nail polish (except for the treatment window) and demineralized for additional days in order to investigate the progression of demineralization with time. The treatment window of sample used in this study is demineralized for up to 10 days and imaging is carried out on the sample at several lock-in modulation frequencies before the treatment as well as after 2 days, 4 days, 6 days, 8 days, and 10 days of treatment.

This demineralization protocol effectively mimics the formation and progression of caries in enamel as commonly encountered in dental practice. Numerous studies carried out using transverse micro-radiography (TMR) have verified the ability of this demineralization protocol to produce a subsurface lesion in enamel with a sound surface layer, the characteristic mineral profile of early dental caries [21–25].

3 Results and Discussion

Unlike opaque materials, light interaction in turbid media (e.g., dental hard tissue) is governed by a strongly coupled diffused photon density and thermal-wave processes [26]. In the case of dental caries, this amounts to enhanced local optical scattering and absorption at caries sites, yielding subsurface thermal-wave sources which contribute

to the infrared detector signal radiometrically according to the following well-known formula [26]:

$$S(l;t) \propto \bar{\mu}_{IR} \int_0^l T(z,t) \exp(-\bar{\mu}_{IR} z) dz \tag{2}$$

Here $\bar{\mu}_{IR}$, l, and $T(z,t)$ are the average infrared absorption coefficient over the detection wavelength bandwidth (MIR: 3 μm to 5 μm, LWIR: 8 μm to 14 μm), caries/absorber depth, and the induced thermal-wave field, respectively.

Careful inspection of Eq. 2 indicates that the radiometric signal registered by the IR detector gets contributions from the thermal-wave field in the form of an exponentially attenuated depth integral with $\bar{\mu}_{IR}$ serving as the attenuation coefficient. As such, the spectral bandwidth of the detector (MIR vs. LWIR) plays an important role in the physical nature of the acquired IR signals. In the case of a MIR TPLI system, $\bar{\mu}_{IR}$ is relatively low (enamel transmittance: MIR = 75 % [7]) which results in direct Plank emission (radiative heat transfer) from subsurface thermal sources (e.g., early caries) in addition to the conductive thermal-wave contribution from the interrogation surface. Such dominant radiative contribution from subsurface thermal sources in the MIR band is carried out at the speed of light, masking the desirable conductive thermal-wave contribution required for generating diagnostic contrast in dental TPLI images. For LWIR TPLI, on the other hand, $\bar{\mu}_{IR}$ is significantly larger than that in the MIR band (enamel transmittance: LWIR = 7 % [7]) which effectively results in attenuation of the instantaneous radiative contribution from the subsurface thermal sources, allowing for registration of pure thermal-wave contributions emanating from the sample surface. As such, dental samples in the LWIR detection band effectively behave as opaque materials, allowing one to perform depth profilometry by controlling the thermal diffusion length (Eq. 3) through the optical modulation frequency.

$$\mu_{th}(f) = \sqrt{\frac{\alpha}{\pi f}} \tag{3}$$

In Eq. 3, μ_{th}, α, and f are thermal diffusion length, thermal diffusivity, and optical modulation frequency, respectively.

3.1 Standard Sample

The phase images of the blind holes (200 μm, 500 μm, and 1500 μm wall thicknesses) in the aluminum sample, obtained at 5 Hz, 10 Hz, and 20 Hz optical excitation modulation frequencies are presented in Fig. 2. The sequence of images suggests that the developed LWIR system is capable of resolving holes at different depths with acceptable resolution. As expected, at a given modulation frequency, as the wall thickness increases the outline and the shape of the holes appear with a lower resolution due to the diffuse nature of heat conduction.

The depth profilometry feature of TPLI can be understood by comparing phase images of Fig. 2 produced at different modulation frequencies (Fig. 2a–c). For a given

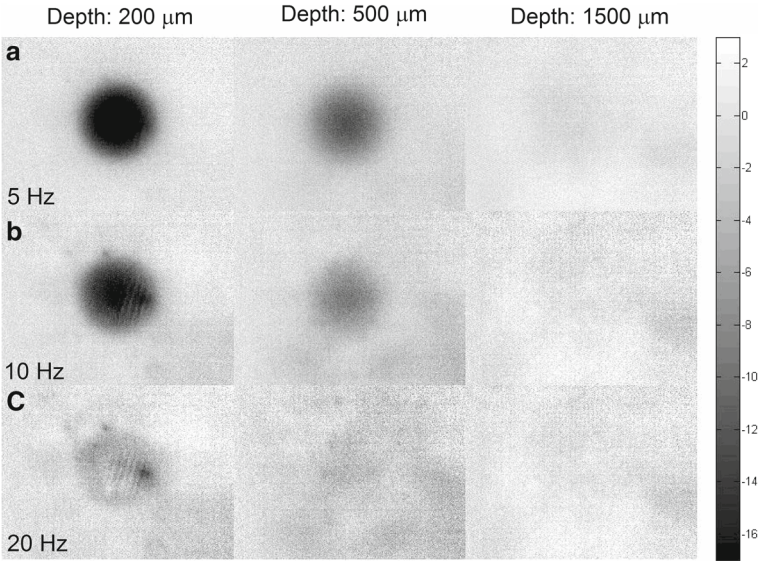

Fig. 2 TPLI phase images of blind holes with different wall thicknesses obtained at (a) 5 Hz, (b) 10 Hz, and (c) 20 Hz optical modulation frequencies, respectively

defect depth, increasing the modulation frequency decreases the thermal diffusion length, leading to a lower effective detection depth and fading of the deeper holes. Consequently, while the intermediate defect (500 μm wall thicknesses) is present in the images at 5 Hz; it fades away by increasing the modulation frequency to 10 Hz and completely disappears at 20 Hz. The results of Fig. 2 clearly demonstrate the expected profilometric feature of thermal waves and serves as a basic validation of the developed LWIR TPLI system.

3.2 Tooth with Artificially Induced Caries

To systematically monitor the progression of demineralization into the enamel, a time-dependent *in vitro* study is carried out. To this end, arrangements should be made to ensure that the sequence of images taken at different times is self-consistent as the optical and thermal properties of teeth slightly change over time, due to the exposure to the surrounding environment. As such, in order to make a valid comparison between a series of phase images taken at different stages of demineralization, a phase normalization method is used [14]. In this method, a relatively healthy area in the tooth is selected (dashed reference area in Fig. 3c), the average phase value of the pixels inside this area is calculated, and eventually the phase values of all the pixels in a given image are subtracted from the average value. This normalization procedure is done for each phase image of a sequence independently using the same location for the reference area. In other words, for a follow-up study, the comparison is made between phase difference images rather than the absolute phase value images. This normalization is the only modification made on the raw phase images of Fig. 3.

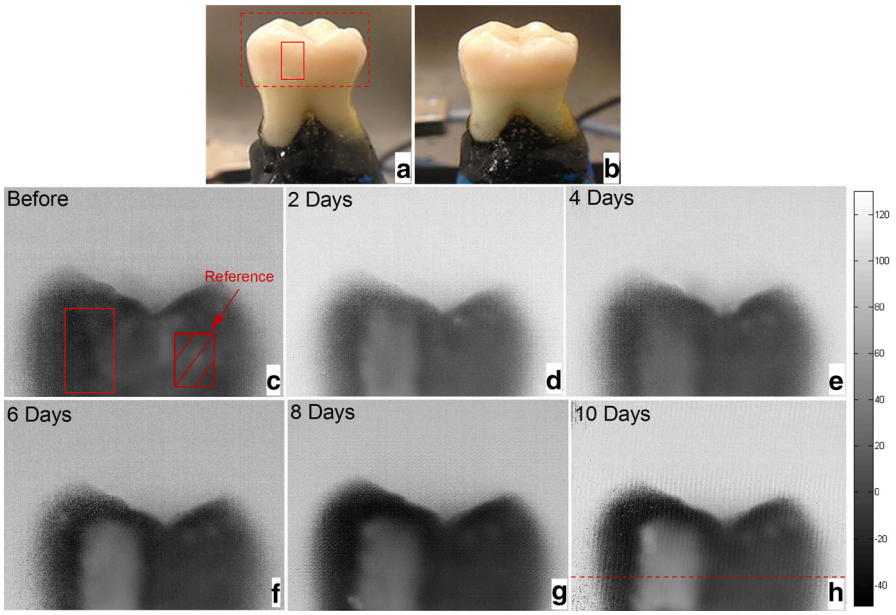

Fig. 3 Photograph of the sample (a) before and (b) after 10 days of demineralization on the treatment window. TPLI phase images of sample (c) before and after (d) 2 days, (e) 4 days, (f) 6 days, (g) 8 days, and (h) 10 days of treatment [27]

Figure 3a, b depicts the photographs of the sample before and after 10 days of demineralization. The dashed rectangle in this figure shows the field of view of the TPLI imaging system, while the solid rectangle depicts the location of the treatment window. Comparison of the two photographs shows no visual indication of mineral loss in the treatment window after 10 days of demineralization, confirming the insensitivity of conventional visual inspection methods to detection of early demineralization. Figure 3c depicts the TPLI phase image obtained at 2 Hz before application of artificial demineralization. No dominant feature/defect is observed in this image. As such, the sample deemed to be reasonably healthy before application of the demineralization protocol.

Figure 3d–h shows the phase images taken at 2, 4, 6, 8, and 10 days of treatment, respectively. It should be noted that the same contrast mapping has been applied to all images of Fig. 3 to ensure the validity of comparison between images. It can be observed that as treatment time increases, the treated window becomes more apparent, while the intact areas in the images appear more or less the same. This monotonic increase in the average phase values is due to the progression of the demineralization into the enamel leading to an increase in the demineralized lesion depth. As the demineralized region's thickness increases, the thermal-wave centroid shifts farther away from the surface, thereby increasing the phase lag between the applied optical excitation and the received infrared response signal.

Figure 4a is a plot of transverse profiles of the phase values at different stages of formation along the dashed line shown in Fig. 3h. The profiles clearly show the

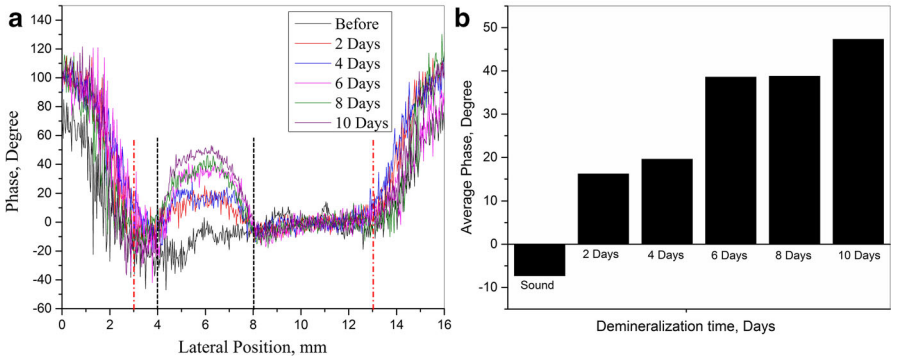

Fig. 4 (a) Phase profiles along the *dashed line* shown in Fig. 3h and (b) average phase values within the treatment window for samples at several demineralization stages [27]

presence of a demineralized region indicated by two vertical dashed lines, representing the location of the treatment window. It can be seen that as demineralization progresses, the thermophotonic phase values increase within the treatment window, while the phase values remain approximately the same at intact regions. The increasing trend in the contrast between treated and untreated areas can be quantitatively validated by comparing the average phase values within the treatment window for the untreated, 2-day, 4-day, 8-day, and 10-day-treated samples which are found to be −7.36°, 16.23°, 19.62°, 38.61°, 38.81°, and 47.35° (Fig. 4b), respectively.

3.3 Tooth with Natural Caries

Figure 5 presents the TPLI amplitude and phase images obtained from a tooth with suspected natural caries at 1 Hz, 5 Hz, and 20 Hz modulation frequencies. Unlike the previous sample, the occlusal surface of this sample is investigated at its natural state (no artificial demineralization protocol is applied). As depicted in the photograph (Fig. 5a), occlusal pit and fissures (e.g., features 1 and 2) can be identified on the occlusal surface of the sample; however, no visual evidence of mineral loss (e.g., white spot lesions) can be observed by visual inspection. Figure 5b, e depicts the TPLI amplitude and phase images obtained at 1 Hz. Features can hardly be resolved in these blurry amplitude and phase images due to the long thermal diffusion length at 1 Hz. At low modulation frequencies, thermal waves face less spatial attenuation and therefore effectively probe deeper into the enamel, yielding superposed contributions from subsurface features within the long thermal diffusion length. To avoid the interfering effects of deep features (supposedly from dentin [14,28]), the thermal diffusion length is reduced by imaging at 5 Hz and 20 Hz to interrogate the clinically relevant near-surface regions of the occlusal surface. A considerable improvement in the axial resolution is clearly evident in both amplitude and phase images obtained at higher frequencies (Fig. 5c, d, f, g).

Features 1 and 2 are healthy-looking occlusal pit and fissures which appear to be demineralized based on the LWIR TPLI amplitude and phase images. The enhanced

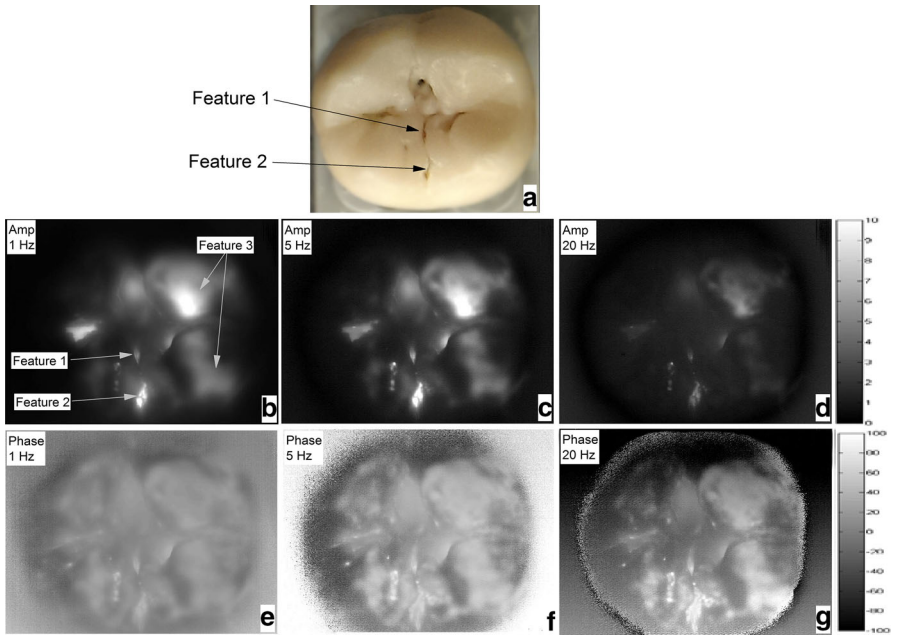

Fig. 5 (a) Photograph of the occlusal surface of the tooth sample. TPLI (b–d) amplitude and (e–g) phase images of the occlusal surface obtained at 1 Hz, 5 Hz, and 20 Hz optical modulation frequencies, respectively

local optical absorption at these caries sites increases the thermal-wave amplitude and shifts the thermal-wave centroid causing the diagnostic contrast in the amplitude and phase images. Comparison of the phase images obtained at different frequencies suggests that features 1 and 2 are perhaps early caries located very close to surface as they appear more resolved in the 20 Hz phase image with the shortest thermal diffusion length (Fig. 5g).

Although the occlusal surface of the tooth (Fig. 5a) looks relatively healthy, appearance of two bright spots in the phase and amplitude images (feature 3 in Fig. 5d, g) suggests the presence of a demineralized area at the occlusal cusps. These early caries also appear to be very close to surface as their shape and outline are revealed only at the highest modulation frequency (Fig. 5e, f vs. 5g). The results obtained from this sample are in agreement with those of Tabatabaei et al. [14] from teeth with natural caries which were verified by TMR.

The obtained results from occlusal surface imaging suggest the potential of the developed LWIR TPLI system in probing natural occlusal caries which is most commonly encountered in the clinical practice. The significance of early detection of occlusal caries lies in the fact that this surface cannot directly be imaged via X-ray radiography. X-ray radiography works based on the transmission of radiation though the enamel and thus, the detector is to be placed beneath the occlusal surface which is not feasible in dental practice. Aside from sensitivity to early demineralization, direct imaging of occlusal surfaces serves as an immediate advantage for the TPLI

system over X-ray radiography to be used as an effective diagnostic tool in clinical applications.

4 Conclusion

This study reports on development of a commercially viable thermophotonic lock-in imaging system for detection of early dental caries using a low-cost LWIR infrared camera. To date, this is the first report on biomedical application of active thermography in the LWIR region. The capabilities of this noncontact, noninvasive diagnostic system are demonstrated through experiments performed on biological and nonbiological samples. The experimental results suggest that the developed inexpensive TPLI system is capable of detecting very early demineralization lesions, impossible to diagnose by visual inspection. This study also suggests that using LWIR TPLI images, one can effectively probe the occlusal surface of tooth which cannot be directly imaged using X-ray radiography. As such, the developed imaging system is a promising candidate of reasonable contrast and sensitivity to carious lesions, very suitable for transition to Dentistry as a commercially and clinically viable diagnostic imaging device.

Acknowledgments We are grateful to the Natural Sciences and Engineering Research Council of Canada for Discovery Grant awarded to N.T. and to Lassonde School of Engineering and York University for their financial support through the institutional start-up grant.

References

1. O. Fejerskov, E.A. Kidd, O.L.E. Fejerskov, E.A. Kidd, *Dental Caries* (Blackwell Munksgaard, Copenhagen, 2003)
2. J.D. Featherstone, Community Dent. Oral **27**, 31 (1999)
3. S.C. White, M.J. Pharoah, *Oral Radiology: Principles and Interpretation* (Elsevier, Philadelphia, 2014)
4. J.D. Bader, D.A. Shugars, A.J. Bonito, J. Public Health Dent. **62**, 201 (2002)
5. D. Fried, C.M. Bühler, P. Ngaotheppitak, C.L. Darling, Proc. J. Biomed. Opt. **6137**, 61370L (2006)
6. C. Zakian, I. Pretty, R. Ellwood, J. Biomed. Opt. **14**, 064047 (2009)
7. J.D. Featherstone, D. Fried, Med. Laser Appl. **16**, 181 (2001)
8. A. Hall, J.M. Girkin, J. Dent. Res. **83**, C89 (2004)
9. B.T. Amaechi, J. Appl. Phys. **105**, 102047 (2009)
10. S. Kaiplavil, A. Mandelis, Nat. Photon. **8**, 635 (2014)
11. C. Meller, C. Heyduck, S. Tranaeus, C. Splieth, Caries Res. **40**, 90 (2006)
12. C. John, A. Salerno, in *Proceedings of the 11th International Symposium Computed Assistant Radiology (CAR97)*, vol. 986 (1997), p. 986
13. C. John, D. Wu, A. Salerno, G. Busse, C. Löst, *Nondestructive Characterization of Materials*, vol. 3 (Springer, New York, 1998), pp. 757–762
14. N. Tabatabaei, A. Mandelis, B.T. Amaechi, J. Biomed. Opt. **16**, 071402 (2011)
15. C. Meola, G.M. Carlomagno, *Nondestructive Testing of Materials and Structures* (Springer, Dordrecht, 2013)
16. G. Giorleo, C. Meola, A. Squillace, Nondestruct. Test. Eval. **16**, 15 (2000)
17. Y.K. An, J.M. Kim, H. Sohn, NDT&E Int. **65**, 54 (2014)
18. C. Meola, V. Grasso, C. Toscano, G.M. Carlomagno, *Residual Stress, Thermomechanics & Infrared Imaging, Hybrid Techniques and Inverse Problems*, vol. 8 (Springer, New York, 2014), pp. 207–213
19. N. Tabatabaei, A. Mandelis, Phys. Rev. Lett. **107**, 165901 (2011)
20. O. Breitenstein, M. LangenKamp, *Lock-In Thermography: Basics and Use for Functional Diagnostics of Electronic Components* (Springer, New York, 2003)
21. B.T. Amaechi, S.M. Higham, W.M. Edgar, Arch. Oral Biol. **43**, 619 (1998)

22. A. Hellen, A. Mandelis, Y. Finer, B.T. Amaechi, J. Biomed. Opt. **16**, 071406 (2011)
23. A. Hellen, A. Mandelis, Y. Finer, J. Phys. Conf. Ser. **214**, 012024 (2010)
24. R.J. Jeon, A. Hellen, A. Matvienko, A. Mandelis, S.H. Abrams, B.T. Amaechi, Proc. J. Biomed. Opt., 68560B (2008)
25. B.T. Amaechi, A.G. Podoleanu, G.N. Komarov, J.A. Rogers, S.M. Higham, D.A. Jackson, Laser Phys. **13**, 703 (2003)
26. A. Mandelis, *Diffusion-Wave Fields: Mathematical Methods and Green Functions* (Springer, New York, 2013)
27. A. Ojaghi, A. Parkhimchyk, N. Tabatabaei, *Proc. SPIE* 9692, Lasers in Dentistry XXII, 969209 (2016)
28. R.J. Jeon, A. Mandelis, V. Sanchez, S.H. Abrams, J. Biomed. Opt. **9**, 804 (2004)